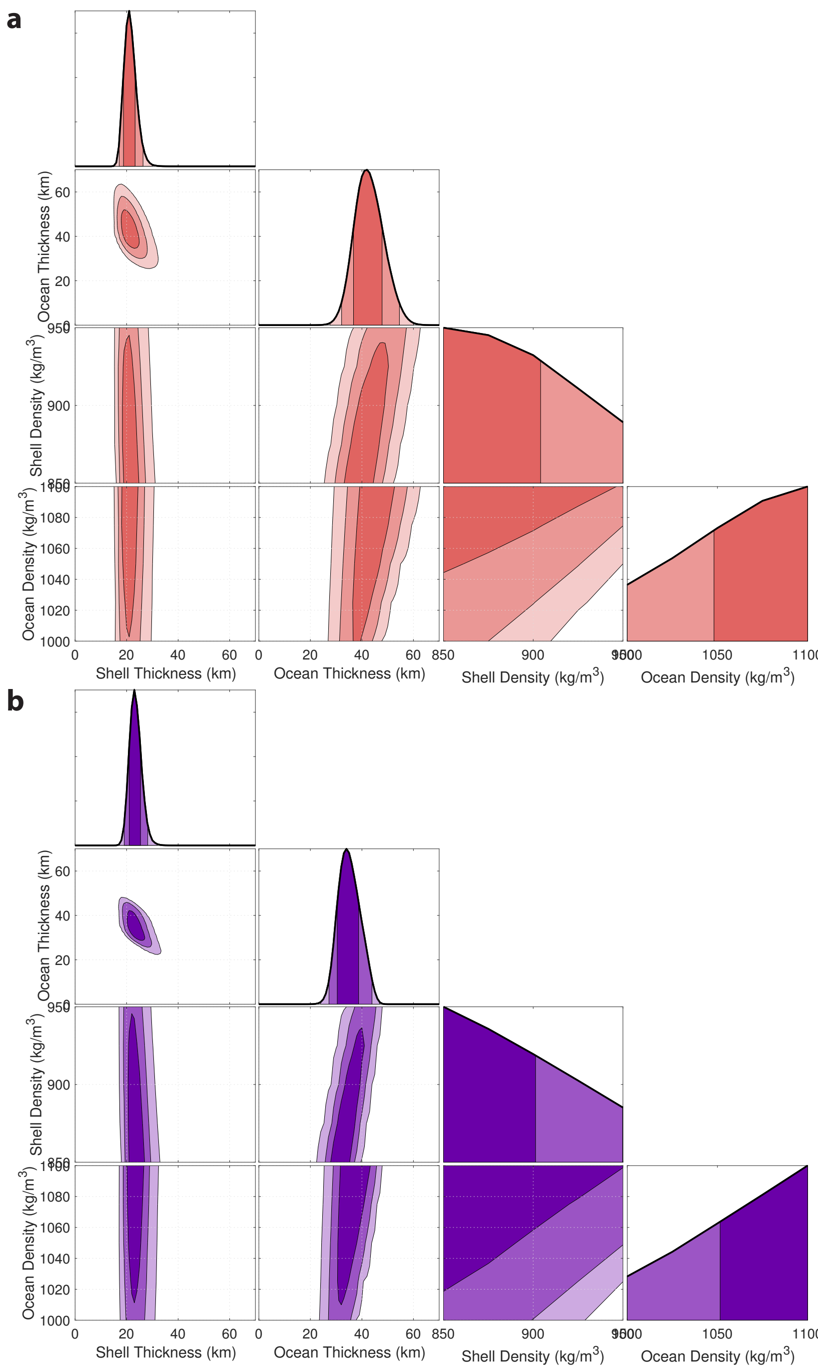

Figure S1: The ranges of model parameters that best account for the observed gravitational potential and libration amplitude, given the shape model of (a) *Nimmo et al.* (2011) or (b) *Tajeddine et al.* (2017), and assuming the topography is supported by Airy isostasy (*Hemingway and Matsuyama*, 2017). Illustrated along the diagonal are the normalized probability density functions across each of the four model parameters. The remaining cells in the grid illustrate the joint probability density function for each pair of parameters. The shaded regions represent 68% (dark), 95% (intermediate), and 99.7% (pale) confidence contours (section 2.6). The minimum misfits are $L = 0.6$ and $L = 3.2$ for the *Nimmo et al.* (2011) and *Tajeddine et al.* (2017) shape models, respectively.

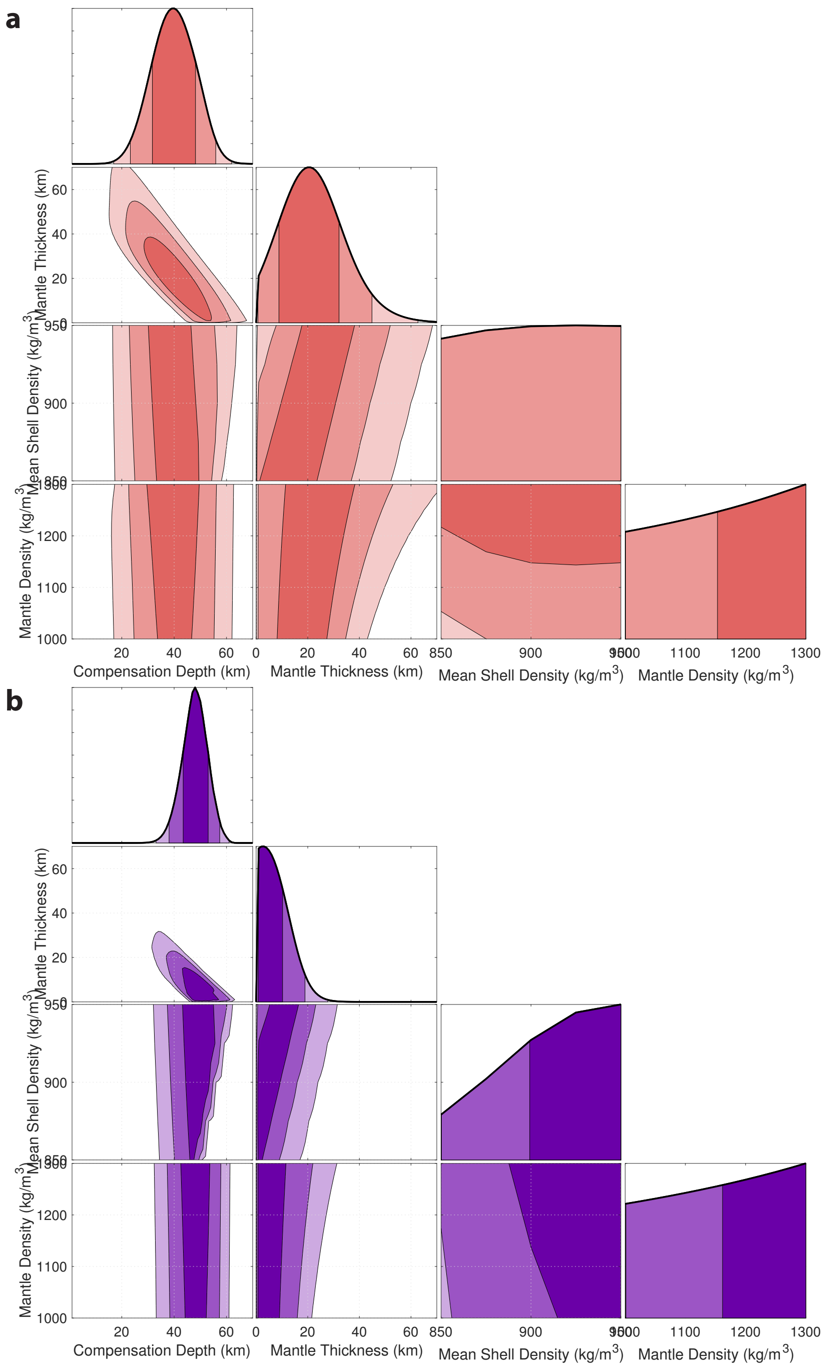

Figure S2: The ranges of model parameters that best account for the observed gravitational potential, given the shape model of (a) *Nimmo et al.* (2011) or (b) *Tajeddine et al.* (2017), and assuming the topography is supported by Pratt isostasy. Illustrated along the diagonal are the normalized probability density functions across each of the four model parameters. The remaining cells in the grid illustrate the joint probability density function for each pair of parameters. The shaded regions represent 68% (dark), 95% (intermediate), and 99.7% (pale) confidence contours (section 2.6). The minimum misfits are $L = 6.0$ and $L = 7.0$ for the *Nimmo et al.* (2011) and *Tajeddine et al.* (2017) shape models, respectively.

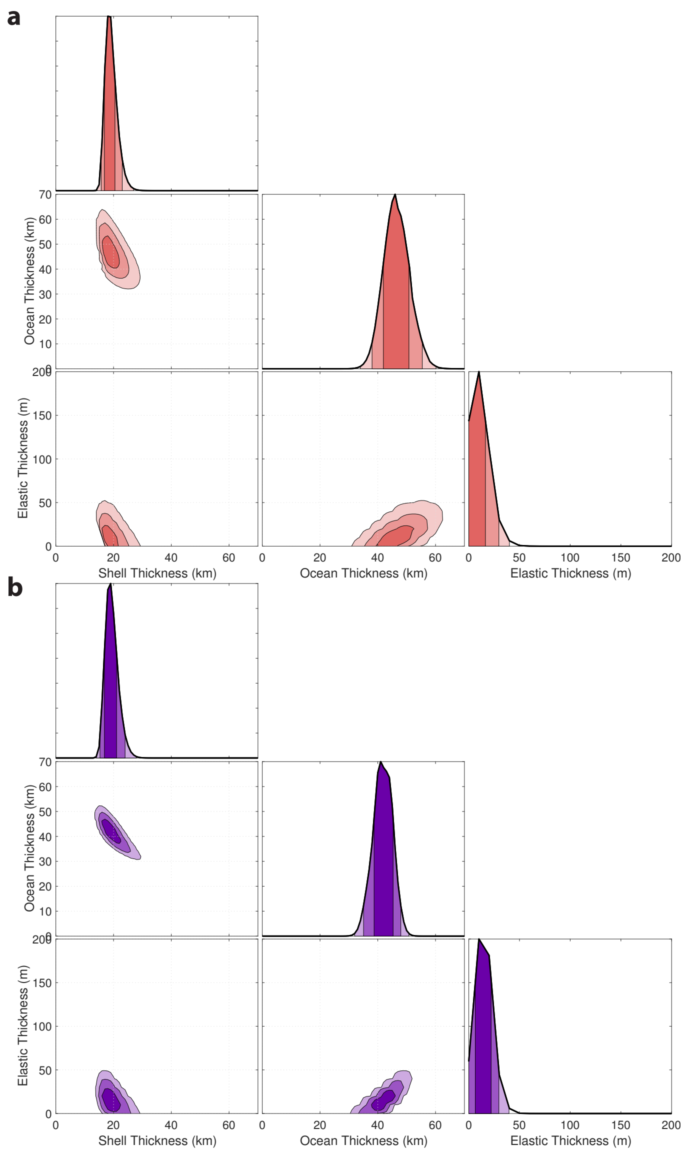

Figure S3: The ranges of model parameters that best account for the observed gravitational potential, given the shape model of (a) *Nimmo et al.* (2011) or (b) *Tajeddine et al.* (2017), and assuming the topography is supported by Airy isostasy plus elastic flexure, assuming top loading. Illustrated along the diagonal are the normalized probability density functions across each of the three model parameters. The remaining cells in the grid illustrate the joint probability density function for each pair of parameters. The shaded regions represent 68% (dark), 95% (intermediate), and 99.7% (pale) confidence contours (section 2.6). The minimum misfits are $L = 0.6$ and $L = 3.3$ for the *Nimmo et al.* (2011) and *Tajeddine et al.* (2017) shape models, respectively.

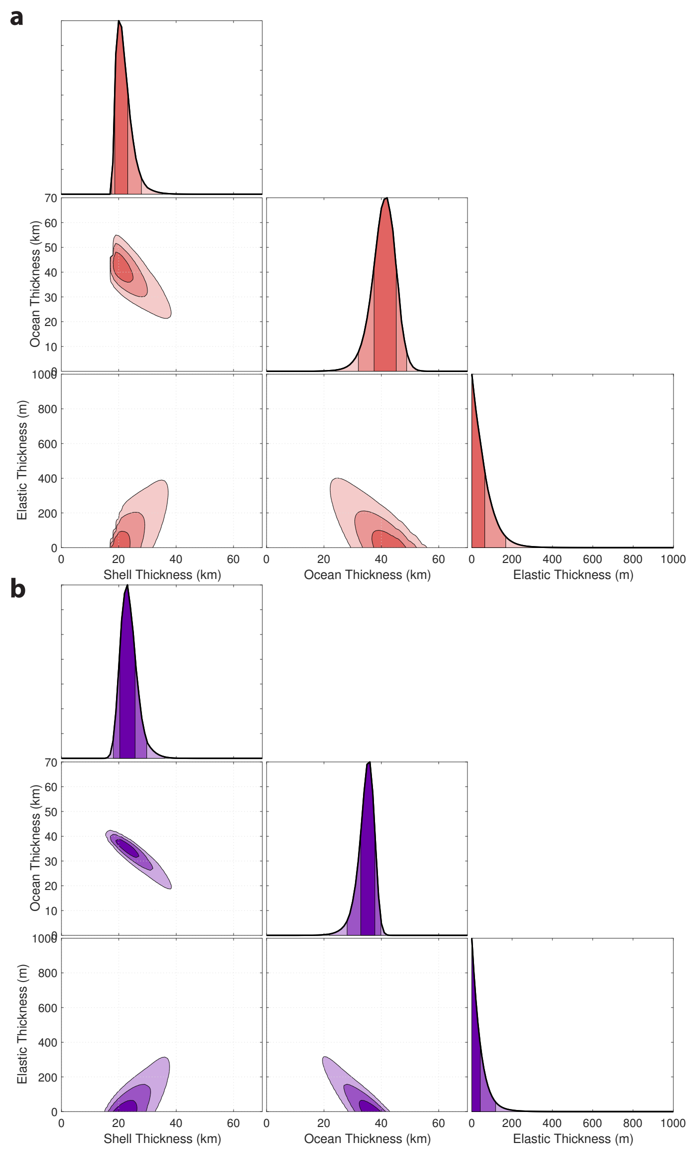

Figure S4: The ranges of model parameters that best account for the observed gravitational potential, given the shape model of (a) *Nimmo et al.* (2011) or (b) *Tajeddine et al.* (2017), and assuming the topography is supported by Airy isostasy plus elastic flexure, assuming bottom loading. Illustrated along the diagonal are the normalized probability density functions across each of the three model parameters. The remaining cells in the grid illustrate the joint probability density function for each pair of parameters. The shaded regions represent 68% (dark), 95% (intermediate), and 99.7% (pale) confidence contours (section 2.6). The minimum misfits are $L = 1.0$ and $L = 3.7$ for the *Nimmo et al.* (2011) and *Tajeddine et al.* (2017) shape models, respectively.

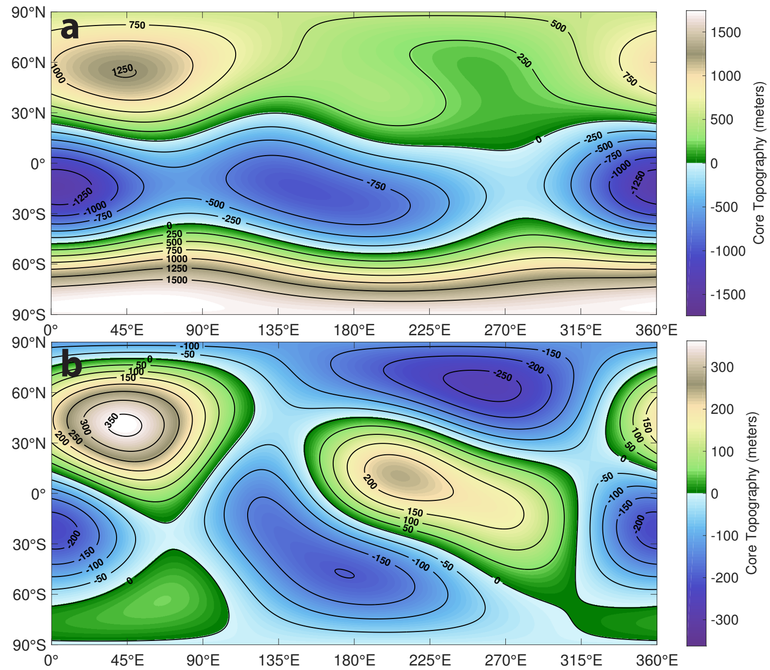

Figure S5: Non-hydrostatic core topography (up to $l = 3$ only) required to satisfy gravity observations perfectly given an external shape described by *Tajeddine et al.* (2017) and assuming (a) no isostatic compensation, such that the ice/ocean interface follows a hydrostatic equilibrium figure; or (b) the topography is supported by Airy isostasy, as in section 3.2.3, such that most of the compensation occurs through deflection of the ice/ocean interface and that the small remaining gravity anomalies are accommodated by non-hydrostatic core topography. In this example case, $d_{\text{shell}} = 21\,\text{km}$, $d_{\text{ocean}} = 37\,\text{km}$, $\rho_{\text{shell}} = 925\,\text{kg/m}^3$, and $\rho_{\text{ocean}} = 1020\,\text{kg/m}^3$.

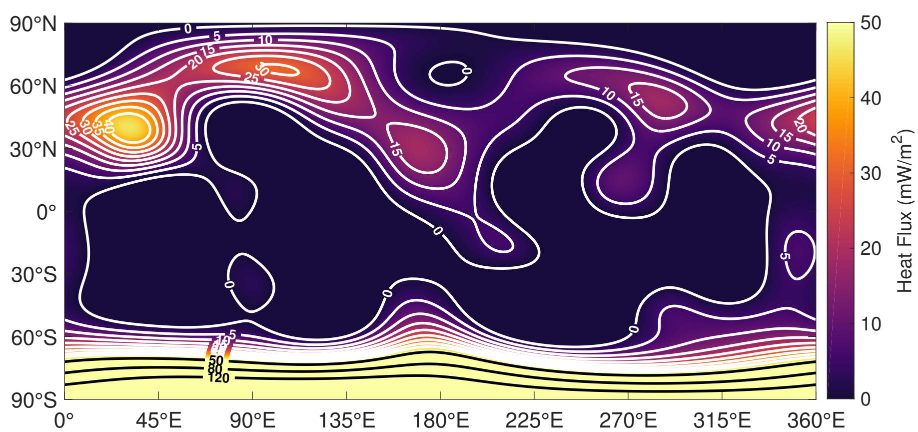

Figure S6: Heat anomaly obtained by subtracting the tidal dissipation model results (Figure 11a) from the inferred heat flux (Figure 11b). Integrated over the surface, the total heat anomaly here is approximately 3 GW.